Springer

KSME

Journal of Mechanical Science and Technology 31 (5) (2017) 2129~2141
www.springerlink.com/content/1738-494x(Print)/1976-3824(Online)
DOI 10.1007/s12206-017-0409-5

Characteristics analysis of aero-engine whole vibration response with rolling bearing radial clearance†

Haifei Wang[1,*], Junjie Gong[1] and Guo Chen[2]

[1]*College of Mechanical Engineering, Yangzhou University, Yangzhou, 225127, China*
[2]*College of Civil Aviation, Nanjing University of Aeronautics and Astronautics, Nanjing, 210016, China*

(Manuscript Received July 7, 2016; Revised November 28, 2016; Accepted January 7, 2017)

Abstract

For the influence of rolling bearing radial clearance on the whole vibration in the aero-engine whole system, a real engine rotor-bearing-casing whole model is established. The rotor and casing systems are modeled by means of FEM; the support systems are modeled by lumped-mass model; rolling bearing radial clearance and strong-nonlinearity of Hertz contact force at four different supports are considered. The coupled system response is obtained by the numerical integral method. The characteristics of the whole vibration response are analyzed. For rolling bearing at a typical support, the rotor, outer ring of rolling bearing and casing response characteristics at different rotating speeds are analyzed. The changing law of contact forces for each ball and the global contact forces at different speeds are analyzed. The influence of the radical clearance on the contact forces on the whole vibration is analyzed. The results show that the contact forces will be larger and the acceleration amplitude jumps obviously when the radial clearance is increased, and due to the variable stiffness of the rolling bearing, the natural frequency will appear when the stiffness changes fiercely, that is *frequency-locked* phenomenon. When the radical clearance is larger and the rotating speed is between two critical speeds, the rotor squeezes the outer ring now and then. Reducing the radical clearance can reduce the whole vibration and increase the rotor's stability.

Keywords: Radial clearance; The whole vibration; The finite model; Hertz contact force; Unbalanced force

1. Introduction

Rolling bearing is an important part in aero-engine. Due to the strong nonlinear characteristics in rolling bearing, it has great influence on the whole vibration response. Scholars at home and abroad have made many studies on the clearance and contact force between the ball and the race. Ehrich [1, 2] studied the dynamics of rotors with bearing clearance. Sinou [3] studied the non-linear dynamic response of a flexible rotor supported by ball bearings by using the Harmonic balance method. Harsha et al. [4, 5] analyzed non-linearity causing the transition from contact to no contact state due to the bearing clearance. Tiwari et al. [6, 7] analyzed the non-linear rotor dynamics numerically and experimentally. Jang et al. [8] studied the vibration due to ball bearing waviness in a rotating system. Chen et al. [9] established a new rotor-support-stator coupling system dynamic model for practical aero-engine considering the nonlinear Hertzian contact force between balls and races, and the varying compliance vibration with rubbing coupling faults. The numerical method was applied to gain responses, and bifurcation and chaotic motions were analyzed. Bai et al. [10] established a general dynamic model with surface waviness. Wu et al. [11] studied the non-synchronous vibration of a Jeffcott rotor due to internal radial clearance in roller bearing.

As can be seen from the current literatures, the existing rolling bearing models are complete, however, considering characteristics analysis of the aero-engine whole vibration response is less. The existing models are based on the simple rotor model; the rolling bearing models are not applied in the real engine model. The ball bearing clearance is considered in the existing results, which leads to nonlinear response of the rotor system, however, the contact force for each ball, the global contact forces on the rolling bearing, and the rotor operation laws are not considered.

In this paper, a real aero-engine whole vibration model is established. The rolling bearing radial clearance is considered in this model. Based on the casing acceleration signal and the rotor displacement signal, the real engine vibration response characteristics are analyzed. The forces of the rolling element and the rotor operation laws under different speeds are analyzed. The influence of the radial clearance on the contact forces on whole vibration is studied.

*Corresponding author. Tel.: +86 18752787983
E-mail address: wanghaifei1986318@163.com
† Recommended by Associate Editor Junhong Park

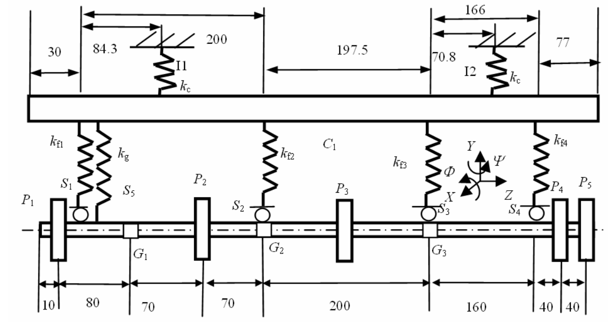

Fig. 1. Rotor-support-casing coupling model of a type of aero-engine (unit: *mm*).

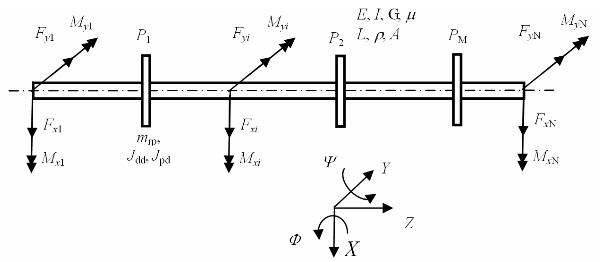

Fig. 2. The finite element rotor model.

2. A dynamic model for certain type aero-engine

2.1 The structure sketch map for certain real engine

A certain real engine model can be referred in Refs. [15, 16]. Its structure is described in detail. Its sketch map is shown in Fig. 1. The symbols in Fig. 1 are described as follows: P_1–P_5 denote different disks; the C_1 denotes the casing; G_1–G_3 denote different gear couplings; S_1–S_4 denote different support point bearings; I_1–I_2 denote different front installation nodes; k_g is the mesh stiffness of a gear pump; k_{f1}–k_{f4} denote different support stiffness; k_c is the connection stiffness.

The rotor-support-casing coupling dynamic model for a real engine is established. Its concrete method for modeling is as follows.

2.2 Dynamics model

2.2.1 Rotor model and casing model

Beam element for rotor model and casing model is established by FEM. The mass, inertias, and gyroscopic moments of the disks are considered in rotor model; however, these parameters are not considered in casing model. The casing model is considered beam element model without considering rotating effect. The finite element rotor dynamic model is shown in Fig. 2.

The symbols in Fig. 2 are described in Ref. [15]. A coordinate system is shown in Fig. 2, and the O-XYZ is a fixed coordinate system, the four vibration directions of the rotor/casing node are considered, that is $\mathbf{q} = [x, y, \varphi, \psi]$. The rotor finite element modeling process can be referred in Ref. [15].

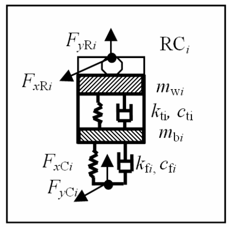

Fig. 3. Rotor-casing support.

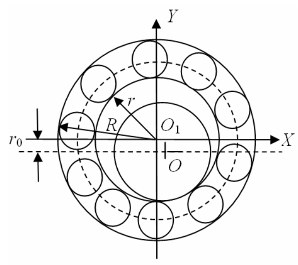

Fig. 4. Rolling bearing model.

The system's motion equation can be obtained, which is:

$$(\mathbf{M}_s)\ddot{\mathbf{q}}_s + (\mathbf{C}_s - \omega \mathbf{G}_s)\dot{\mathbf{q}}_s + \mathbf{K}_s \mathbf{q}_s = \mathbf{Q}_s \tag{1}$$

where $\mathbf{Q}_s$ is the external force vector; $\mathbf{M}_s$ is the mass matrix; $\mathbf{G}_s$ is gyroscopic matrix; K_s is the stiffness matrix; $\mathbf{C}_s$ is the damping matrix.

In this paper, $\mathbf{C}_s = \alpha_0 \mathbf{M}_s + \alpha_1 \mathbf{K}_s$, of which, α_0 and α_1 are supposed to be constants.

The coupling connection between rotors, and Elastic support between casing and base modeling can be referred in Ref. [15].

2.2.2 Discrete support model

The connection modeling between rotor and casing can be referred in Ref. [15]. Suppose that, m_{wi} is the outer bearing mass; m_{bi} is the bearing housing mass; k_{ti} is the support stiffness; c_{ti} is the damping coefficient; k_{fi}, c_{fi} are respectively the support stiffness and damping coefficient. As shown in Fig. 3, F_{yRi} and F_{xRi} are the force of rotor acting on the support RC_i, and the F_{yCi} and F_{xCi} are the force of casing acting on support RC_i. In this section, the modeling process of rolling bearings is described in detail.

The rolling bearing model is shown in Fig. 4, when the ball bearing works, with the contact position periodically varying, the total stiffness and compliance of the bearing will periodically vary, and the Varying compliance (VC) of the bearing is a parametric excitation of a rotor-balling bearing coupling system, finally, a so-called VC vibration is generated. VC vibration is an inherent vibration. it always exists even if the bearing is new and does not have any faults.

Assume the displacements of the mth node of rotor are x_{Rm} and y_{Rm}, let $x = x_{Rm} - x_{wi}$, $y = y_{Rm} - y_{wi}$, according to Chen et al. [13], the ball force can be expressed as:

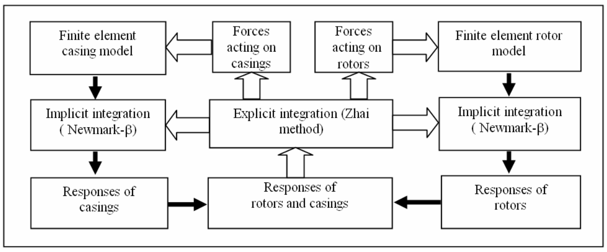

Fig. 5. Solving flow for rotor-support-casing coupling dynamics.

$$\begin{cases} F_{\mathrm{xRi}} = \sum_{j=1}^{N} C_{\mathrm{b}} (x\cos\theta_j + y\sin\theta_j - r_0)^{3/2} \mathrm{H}(x\cos\theta_j + y\sin\theta_j - r_0)\cos\theta_j \\ F_{\mathrm{yri}} = \sum_{j=1}^{N} C_{\mathrm{b}} (x\cos\theta_j + y\sin\theta_j - r_0)^{3/2} \mathrm{H}(x\cos\theta_j + y\sin\theta_j - r_0)\sin\theta_j \end{cases}. \tag{2}$$

In the formula, C_{b} is the Hertzian contact stiffness and $\mathrm{H}(\bullet)$ is the Heaviside function. θ_j is the jth ball's angle position, that is $\theta_j = \omega_{\mathrm{Cage}} \times t + \frac{2\pi}{N_{\mathrm{b}}}(j-1),\ j = 1,2,\cdots N_{\mathrm{b}}$, where, N_{b} is the number of balls. ω_{Cage} is the cage's speed. Suppose the outer race radius is R, the inner ring radius is r, $\omega_{\mathrm{Cage}} = \frac{\omega \times r}{R + r}$, and the ω is shaft rotating angular velocity.

Because the inner race is fixed to the shaft, $\omega_{\mathrm{inner}} = \omega_{\mathrm{rotor}}$. If N_{b} is the number of balls, then VC frequency can be given by

$$\omega_{\mathrm{vc}} = \omega_{\mathrm{Cage}} \times N_{\mathrm{b}} = \omega_{\mathrm{Rotor}} \times B_{\mathrm{N}} \tag{3}$$

where $B_N = N_{\mathrm{b}} \times r/(R+r)$. Obviously, the number B_N depends on the bearing size. In this paper, $B_{N1} = 5.5$, $B_{N2} = 4.85°$.

The bearing outer race's differential equation is

$$\begin{cases} m_{\mathrm{wi}}\ddot{x}_{\mathrm{wi}} + k_{\mathrm{ti}}(x_{\mathrm{wi}} - x_{\mathrm{bi}}) + F_{dxi} = F_{\mathrm{xRi}} \\ m_{\mathrm{wi}}\ddot{y}_{\mathrm{wi}} + k_{\mathrm{ti}}(y_{\mathrm{wi}} - y_{\mathrm{bi}}) + F_{dyi} = F_{\mathrm{yRi}} - m_{\mathrm{wi}}g \end{cases} \quad i = 1,2,\cdots N \tag{4}$$

where F_{dxi} and F_{dyi} are damping forces, suppose the damping is viscous, then,

$$F_{dxi} = c_{\mathrm{ti}}(\dot{x}_{\mathrm{wi}} - \dot{x}_{\mathrm{bi}}), \quad F_{dyi} = c_{\mathrm{ti}}(\dot{y}_{\mathrm{wi}} - \dot{y}_{\mathrm{bi}}). \tag{5}$$

2.3 Solution of rotor-support-casing model

The solution can be referred in Ref. [15], which is shown in Fig. 5. The support looseness is considered between bearing housing and casing in Ref. [15], however, the rolling bearing radial clearance is considered at different supports in this paper. The merits of combination method have: The enormous matrix need not to be formed, therefore, the computation efficiency is improved greatly.

Table 1. Unit number of rotors and casings.

Fan rotor	Compressor rotor	Turbine rotor	Casing
11	10	11	24

Table 2. Parameters of rotors.

Parameters	Disk P_1	Disk P_2	Disk P_3	Disk P_4	Disk P_5
Mass m_{p} (kg)	3.88	1.41	5.17	10.28	10.28
Cross-polar inertia J_{pd} (kg·m^2)	0.03	0.003	0.03	0.05	0.05
Cross-equator inertia J_{dd} (kg·m^2)	0.015	0.0015	0.015	0.025	0.025

Table 3. Parameters of fan rotor.

Number	Coordinate/mm	Outer diameter/mm	Inner diameter/mm
1	0	30	0
2	30	48	0
3	71	30	0
4	90	30	0
5	114	36	0
6	162.6	24	0
7	230	24	0

Table 4. Parameters of compressor rotor.

Number	Coordinate/mm	Outer diameter/mm	Inner diameter/mm
1	230	37.6	24
2	248.5	37.6	24
3	286.5	37.6	24
4	307.5	37.6	24
5	329.5	37.6	24
6	374.5	37.6	24
7	408.5	37.6	24
8	427.5	37.6	24

Table 5. Parameters of turbine rotor.

Number	Coordinate/mm	Outer diameter/mm	Inner diameter/mm
1	427.5	30	18
2	463.5	49	36.9
3	593.5	49	36.9
4	625.5	49	36.9
5	670.5	49	36.9

3. The whole vibration simulation with the radial clearance

3.1 Dynamic parameters

The parameters of the rotor, the casing and the connection parameters of system are shown in Tables 1-13. Mass of out ring m_{w} is 0.2 kg, and Bearing carrier mass m_{b} is 10 kg.

Table 6. Parameters of rotors.

Elastic modulus E (Pa)	Density ρ (kg/m^3)	Poisson's ratio μ	Proportion damping ratio α_0	Proportion damping ratio α_1
2.07×10^{11}	7.8×10^3	0.3	5	1.35×10^{-5}

Table 7. Parameters of casing.

Number	Coordinate/mm	Outer diameter/mm	Inner diameter/mm
1	0	260	230
2	200	260	230
3	360	260	230
4	526	260	230
5	670.5	260	230

Table 8. Parameters of casings.

Elastic modulus E (Pa)	Density ρ (kg/m^3)	Poisson's ratio μ	Proportion damping ratio α_0	Proportion damping ratio α_1
2.07×10^{11}	7.8×10^3	0.3	5	1.35×10^{-5}

Table 9. Parameters of ball bearing.

Rolling bearing	Outer race-way radius R/mm	Inner race-way radius r/mm	Ball number N_b	Contact s tiffness C_b/(N/m$^{3/2}$)	Bearing clearance r_0/um
S_1	39.5	29	13	12.4×10^9	0
S_2	39.5	29	13	12.4×10^9	0
S_3	32	17	14	11.9×10^9	0
S_4	32	17	14	11.9×10^9	0

Table 10. Support parameters of rotor-casing.

Sup-ports	Node of rotor	Casing (node)	k_t (N/m)	c_t (N.s/m)	k_f (N/m)	c_f (N.s/m)
RC_1	3	2	1×10^8	2000	1×10^8	1000
RC_2	1	9	1×10^8	2000	1×10^8	1000
RC_3	11	16	1×10^8	2000	1×10^8	1000
RC_4	8	22	1×10^8	2000	1×10^8	1000

Table 11. Collection parameters of rotor-casing.

Collection	Node of rotor	Casing (node)	k_{gx} (N/m)	c_{gx} (N·s/m)	k_{gy} (N/m)	c_{gy} (N·s/m)
RK_1	6	4	1×10^8	0	1×10^8	0

Table 12. Collection parameters of casing-base.

Supports	Node of rotor	Casing (node)	k_t (N/m)	c_t (N.s/m)	k_f (N/m)
CB_1	8	1×10^9	1×10^5	2000	0
CB_2	23	1×10^9	1×10^5	2000	0

Table 13. Coupling parameter between two rotors.

Collection	k_{Rr}/ (N/m)	$k_{R\alpha}$/ (N·m/rad)	c_{Rr} (N·s/m)	$c_{R\alpha}$ (N·m ·s/rad)
RRC_1	1×10^8	1×10^4	2000	0
RRC_2	1×10^8	1×10^4	2000	0
RRC_3	1×10^8	1×10^4	2000	0

3.2 Calculation condition

(1) The radial clearances at the supports S_1, S_2, S_3 and S_4 are considered.

(2) The output is the casing acceleration response and the vibration displacement response at the supports S_1, S_2, S_3 and S_4.

(3) The rotating speed range is 5000-40000 rpm.

3.3 The critical speed analysis under different radical clearances

Figs. 6(a)-(d) show the amplitude-speed curves of the casing lateral acceleration at the ninth node at different supports S_1, S_2, S_3 and S_4 under different radical clearances that is 0 μm, 10 μm, 30 μm and 50 μm. As can be seen from the figures, the first three order critical speeds are 16100 rpm, 20600 rpm and 33800 rpm, respectively. Figs. 6(b)-(d) show the clearances has little influence on the casing response. In Fig. 6(a), At the support S_1, when the clearance is large, the amplitude jumping phenomenon is obvious; when the rotating speed is close to the second order critical speed, the unbalance force plays a major role and the nonlinearity is less, so the amplitude jumping phenomenon is less obvious; when the rotating speed is near the third order critical speed, the nonlinearity plays a major role and the unbalance force is less, so the amplitude jumping phenomenon is obvious. Fig. 7 is the enlargement of Fig. 6(a). Fig. 8 is the result of Ref. [17]. Figs. 7 and 8 show the obvious amplitude jumping phenomenon, which is caused by the strength of nonlinearity of rolling bearing.

3.4 Calculating modal analysis

The first node of fan rotor is applied the lateral transient force 100 N, and the frequency response of the casing lateral acceleration is obtained, which is used to simulate hammering method, as shown in Fig. 9.

3.5 Casing-rotor response characteristics at different rotating speeds

Figs. 10(a)-(e) show the cascade plot of the support S_1, S_2, S_3 and S_4 lateral acceleration response at different rotating speeds with the clearances 30 μm, 30 μm, 30 μm and 30 μm, respectively. In these figures, the frequency changing in the cascade plot of the support S_1 is not obvious; the second order natural frequency f_{n2}, the sixth order natural frequency f_{n6} and the combined frequency of rotational frequency and the sec-

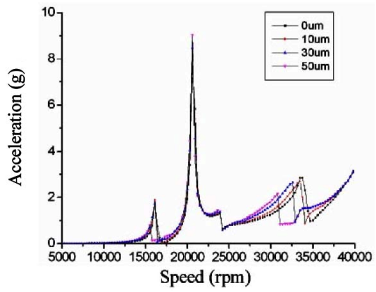

(a) The casing lateral acceleration at the support S_1

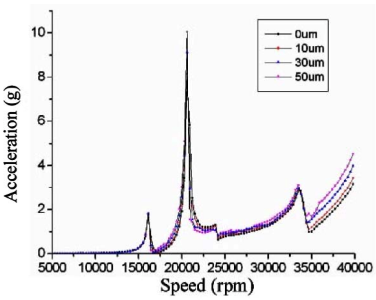

(b) The casing lateral acceleration at the support S_2

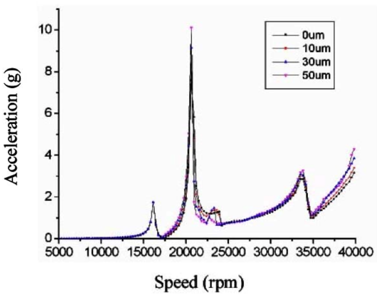

(c) The casing lateral acceleration at the support S_3

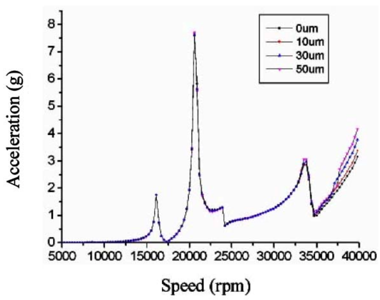

(d) The casing lateral acceleration at the support S_4

Fig. 6. Amplitude-speed curve of casing acceleration response under different clearances at different supports.

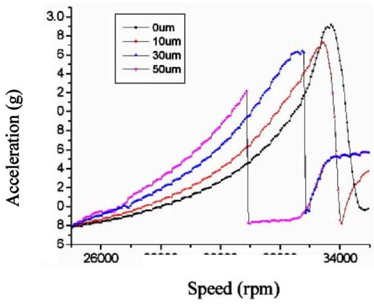

Fig. 7. The enlargement of Fig. 6(a).

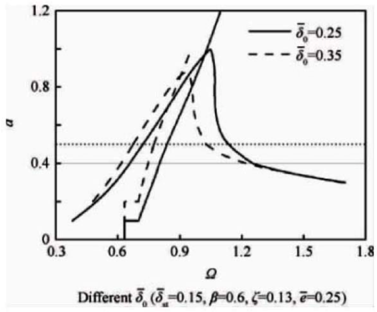

Fig. 8. Result of Ref. [17].

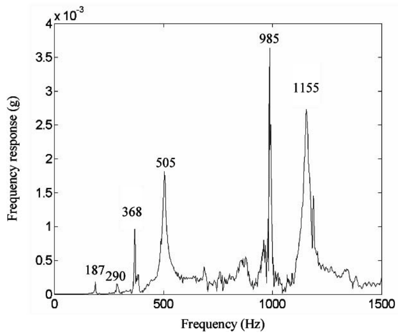

Fig. 9. Frequency response at the ninth node of the casing.

ond order natural frequency f_{n2} appear in the cascade plot of the support S_2; the same phenomenon is in the cascade plot of the support S_3; the sixth order natural frequency f_{n6} appears in the cascade plot of the support S_4. The phenomenon is called *whirl phenomenon* or *frequency-locked phenomenon*. The whip has a constant frequency not depending on the rotating speed [17]. Fig. 11 is from Ref. [17].

Figs. 12(a)-(d) show the bifurcation diagram of the rotor displacements at different supports. In these figures, when the rotating speed is near the critical speed, the bifurcation diagram at different supports shows periodic motion; when the rotating speed is far away from the critical speed, different levels of quasi-periodic and chaotic motion appear; when the rotating speed is higher than the second order critical speed at the supports S_1 and S_2, the phenomenon of quasi-periodic and chaotic motion is obvious.

3.6 Orbits of rotor-out ring and characteristics of casing response at typical rotating speeds

Rotor and casing response characteristics at the support S_2 with the radial clearance 30 μm are analyzed at different speeds, which reveal the rotor operation law and casing response characteristics.

Figs. 13(a)-(d) show the orbits of the rotor and out ring, the bifurcation diagram of the rotor, the wave and frequency

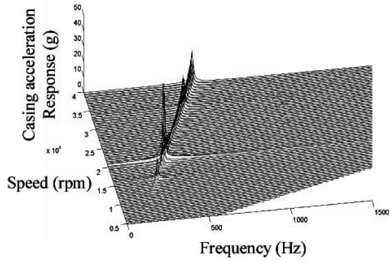

(a) Cascade plot of the casing acceleration response at different speeds without regard to the radical clearance

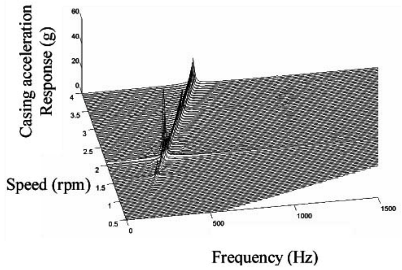

(b) Cascade plot of the casing acceleration response at different speeds considering the radical clearance of the S_1

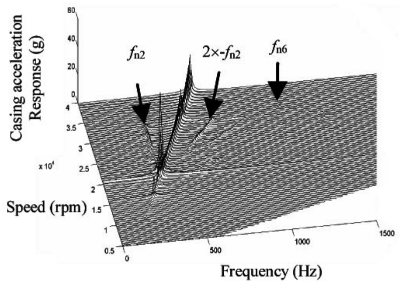

(c) Cascade plot of the casing acceleration response at different speeds considering the radical clearance of the S_2

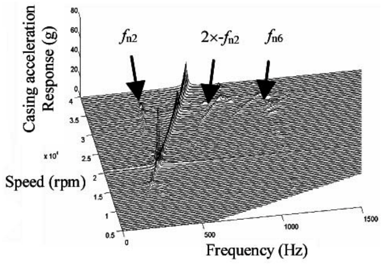

(d) Cascade plot of the casing acceleration response at different speeds considering the radical clearance of the S_3

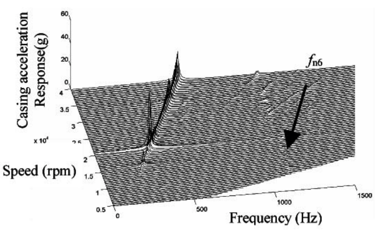

(e) Cascade plot of the casing acceleration response at different speeds considering the radical clearance of the S_4

Fig. 10. Cascade plot of casing acceleration response with radial clearance at different supports.

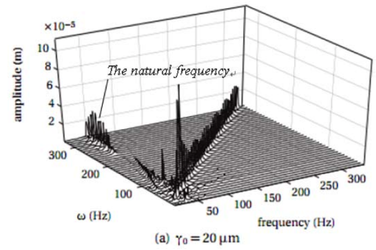

Fig. 11. The result of Ref. [11].

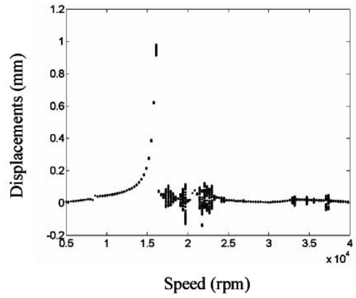

(a) Bifurcation diagram at the support S_1

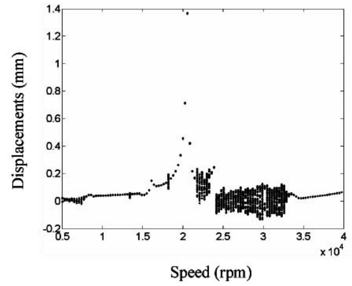

(b) Bifurcation diagram at the support S_2

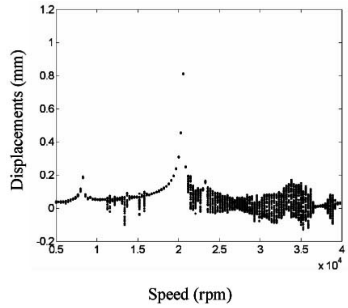

(c) Bifurcation diagram at the support S_3

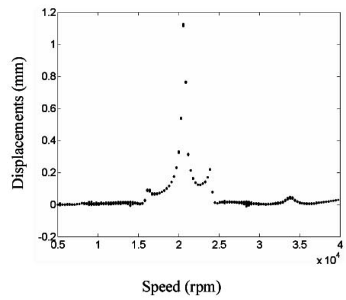

(d) Bifurcation diagram at the support S_4

Fig. 12. Bifurcation diagram of the rotor displacements at different supports.

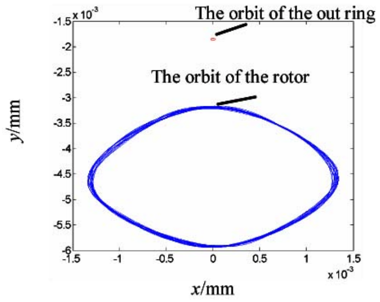

(a) The orbits of the rotor and out ring

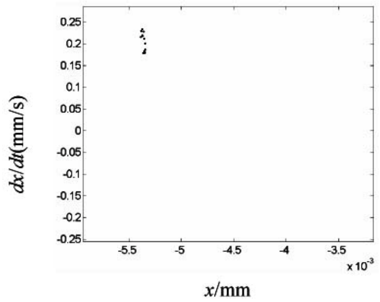

(b) The bifurcation diagram of the rotor

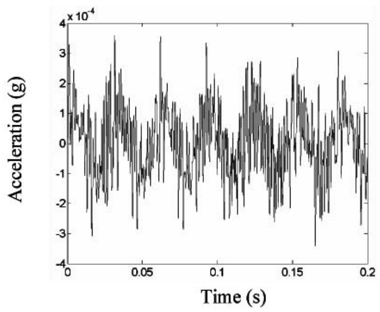

(c) Wave of the casing acceleration

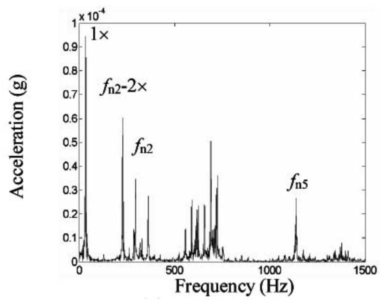

(d) Frequency spectrum

Fig. 13. Orbits of rotor-outer ring, bifurcation diagram of the rotor and wave and spectrum of casing acceleration when the rotating speed is 2000 rpm.

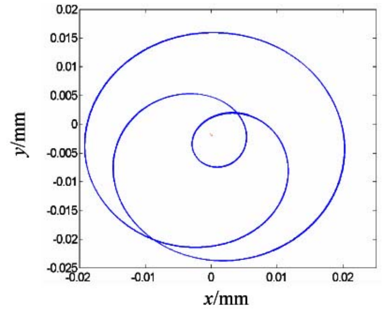

(a) The orbits of the rotor and out ring

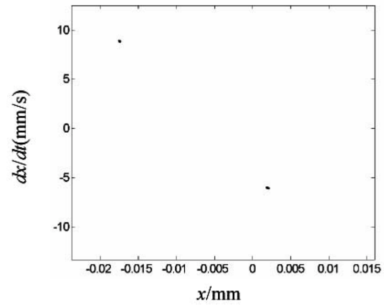

(b) The bifurcation diagram of the rotor

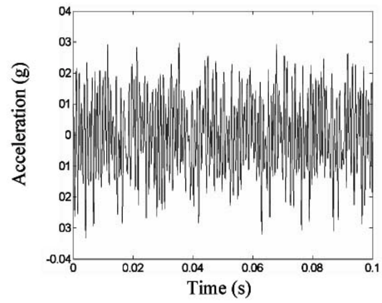

(c) Wave of the casing acceleration

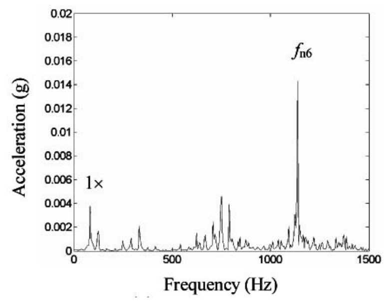

(d) Frequency spectrum

Fig. 14. Orbit of rotor-outer ring, bifurcation diagram of the rotor and wave and spectrum of casing acceleration when the rotating speed is 5000 rpm.

spectrum of casing acceleration at the compressor rotor support S_2 when the rotating speed is 2000 rpm. In Fig. 13(a), due to the effect of many supports and the larger radial clearance, the compressor rotor is whirling at the bottom of the rolling bearing, so the out ring is not squeezed. In Fig. 13(b), the rotor shows weak chaotic motion; In Figs. 13(c) and (d), the rotational frequency, the combined frequency of frequency multiplication and the second order natural frequency f_{n2} appear in frequency spectrum; the sixth order natural frequency f_{n6} appears in high frequency.

Figs. 14(a)-(d) show the orbits of the rotor and out ring, the bifurcation diagram of the rotor, the wave and frequency spectrum of casing acceleration at the compressor rotor support S_2 when the rotating speed is 5000 rpm. In Fig. 14(a), the

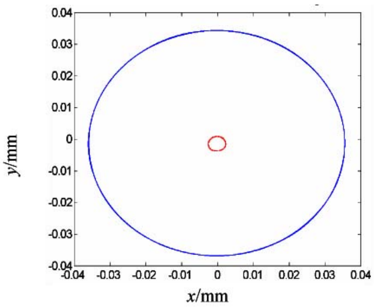

(a) The orbits of the rotor and out ring

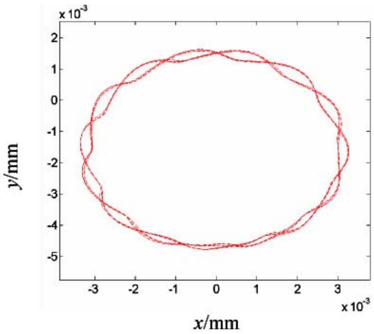

(b) The orbit of the out ring

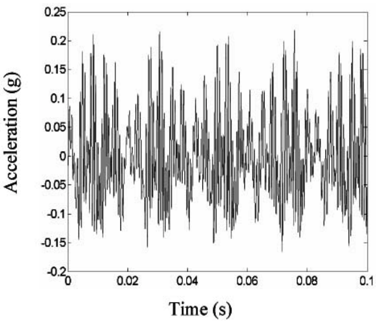

(c) Wave of the casing acceleration

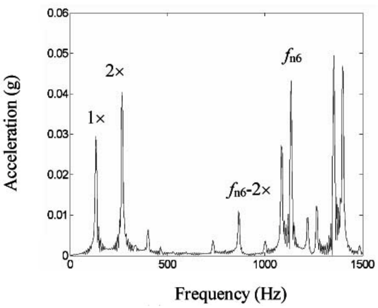

(d) Frequency spectrum

Fig. 15. Orbits of rotor-outer ring, and wave and frequency spectrum of casing acceleration when the rotating speed is 8000 rpm.

compressor rotor is squeezing the out ring. In Fig. 14(b), the rotor shows period-doubling motion; in Figs. 14(c) and (d), the rotational frequency, frequency multiplication and the sixth order natural frequency f_{n6} appear in frequency spectrum.

Figs. 15(a)-(d) show the orbits of the rotor and out ring, the wave and frequency spectrum of casing acceleration at the compressor rotor support S_2 when the rotating speed is 8000 rpm. In Figs. 15(a) and (b), the compressor rotor is squeezing the out ring and whirling along the race, and because the contact force is large, the vibration of the out ring is big, which appear like wavy shape. In Figs. 15(c) and (d), the rotational frequency, the combined frequency of frequency multiplication and the sixth order natural frequency f_{n6} appear in frequency spectrum; the fifth order natural frequency f_{n6} appears in high frequency.

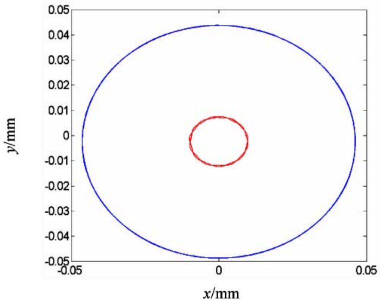

(a) The orbits of the rotor and out ring

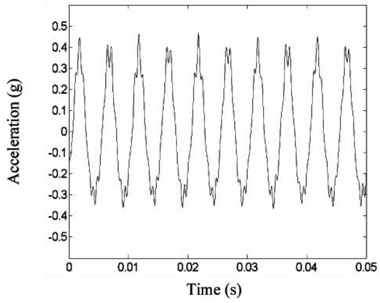

(b) Wave of the casing acceleration

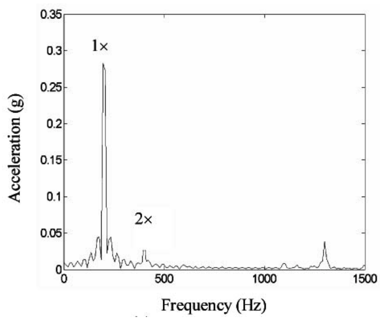

(c) Frequency spectrum

Fig. 16. Orbits of rotor-outer ring, and wave and frequency spectrum of casing acceleration when the rotating speed is 12000 rpm.

Figs. 16(a)-(c) show the orbits of the rotor and out ring, the wave and frequency spectrum of casing acceleration at the compressor rotor support S_2 when the rotating speed is 12000 rpm. In Fig. 16(a), the compressor rotor is squeezing the out ring and whirling along the race, and because the contact force is larger, the vibration of the out ring is bigger. In Figs. 16(b) and (c), the rotational frequency and the VC1 frequency which is B_{N1} times of the rotating frequency, appear in frequency spectrum.

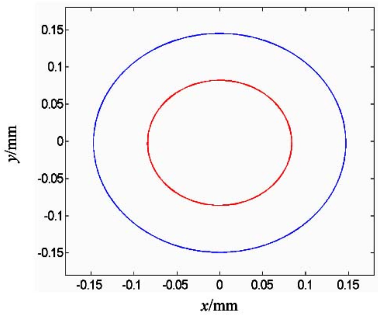

(a) The orbits of the rotor and out ring

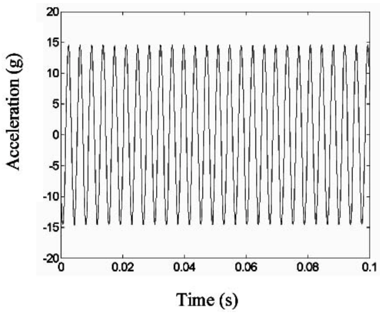

(b) Wave of the casing acceleration

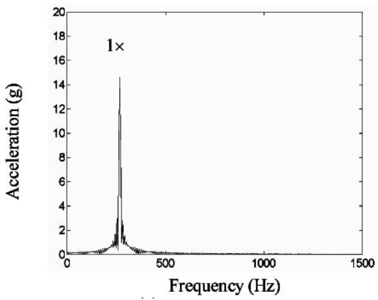

(c) Frequency spectrum

Fig. 17. Orbits of rotor-outer ring, and wave and frequency spectrum of casing acceleration when the rotating speed is 16100 rpm.

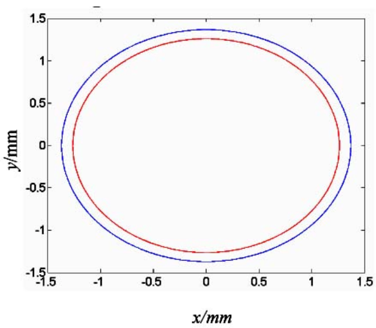

Fig. 18. Orbits of rotor and outer ring when the rotating speed is 20600 rpm.

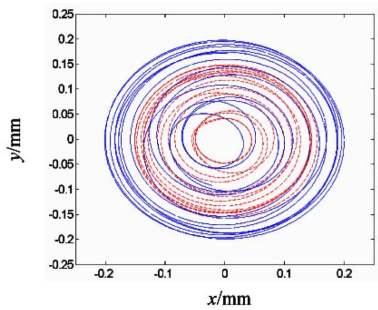

(a) The orbits of the rotor and out ring

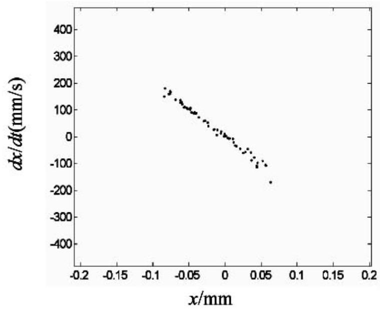

(b) The bifurcation diagram of the rotor

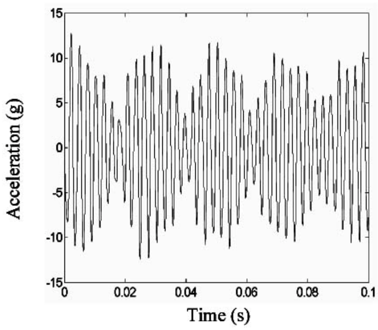

(c) Wave of the casing acceleration

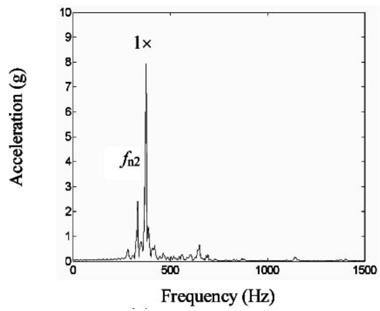

(d) Frequency spectrum

Fig. 19. Orbits of rotor-outer ring, bifurcation diagram of the rotor and wave and spectrum of casing acceleration when the rotating speed is 22500 rpm.

Figs. 17(a)-(c) show the orbits of the rotor and out ring, the wave and frequency spectrum of casing acceleration at the compressor rotor support S_2 when the rotating speed is 16100 rpm, that is, the first order critical speed. In Fig. 17(a), the compressor rotor is squeezing the out ring and whirling along the race, and because the contact force is larger, the vibration of the out ring is bigger, which appears like ellipsoid. In Figs. 17(b) and (c), when the rotating speed is about the first order critical speed, because the unbalanced force is bigger, the rotational frequency appears in frequency spectrum.

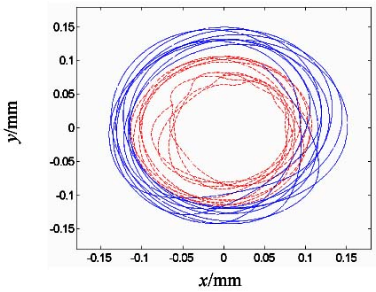

(a) The orbits of the rotor and out ring

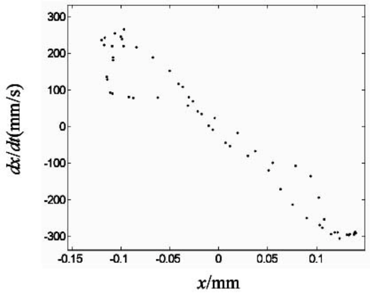

(b) The bifurcation diagram of the rotor

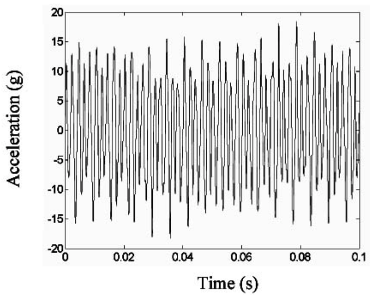

(c) Wave of the casing acceleration

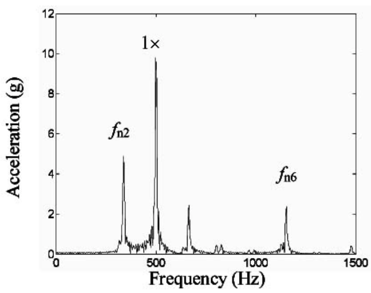

(d) Frequency spectrum

Fig. 20. Orbits of rotor-outer ring, bifurcation diagram of the rotor and wave and spectrum of casing acceleration when speed is 30000 rpm.

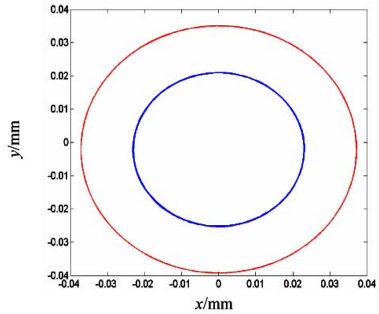

(a) The orbits of the rotor and out ring

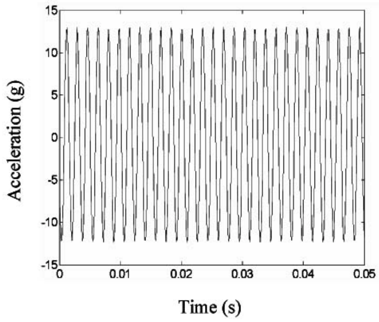

(b) Wave of the casing acceleration

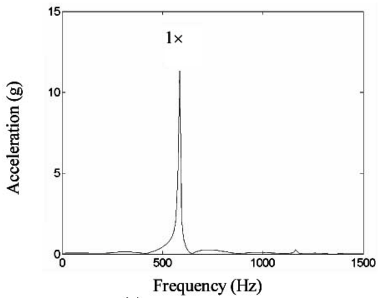

(c) Frequency spectrum

Fig. 21. Orbits of rotor-outer ring, and wave and spectrum of casing acceleration when the rotating speed is 35000 rpm.

Fig. 18 shows the orbits of the rotor and out ring at the compressor rotor support S_2 when the rotating speed is 20600 rpm, that is, the second order critical speed. In Fig. 18, because the unbalanced force continues to increase, the vibration of out ring is further increase.

Figs. 19(a)-(d) show the orbits of the rotor and out ring, the bifurcation diagram of the rotor, the wave and frequency spectrum of casing acceleration at the compressor rotor support S_2 when the rotating speed is 22500 rpm. In Fig. 19(a), the orbits of the rotor and the out ring appear overlap, that is, the rotor squeezes or doesn't squeezes the out ring now and then. In Fig. 19(b), the bifurcation diagram of the rotor appears like a cloud, that is, chaotic motion. In Figs. 19(c) and (d), because the rotational frequency is near the corresponding frequency of the second order critical speed, the continuous spectrum appears, and the wave of the casing acceleration appears beat vibration phenomenon. Due to the instability of the rotor, the stiffness variation fiercely, the second order natural frequency f_{n2} is excited.

Figs. 20(a)-(d) show the orbits of the rotor and out ring, the bifurcation diagram of the rotor, the wave and frequency spectrum of casing acceleration at the compressor rotor support S_2 when the rotating speed is 30000 rpm. In Fig. 20(a), after the rotating speed passed the second order critical speed, due to the larger speed, the contact force increases, the vibration of the out ring is bigger. In Fig. 20(b), the bifurcation diagram of the rotor appears closed loop, that is, chaotic mo-

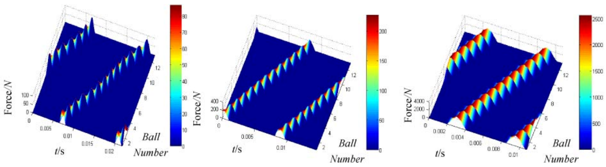

(a) 8000 rpm (b) 12000 rpm (c) 16100 rpm

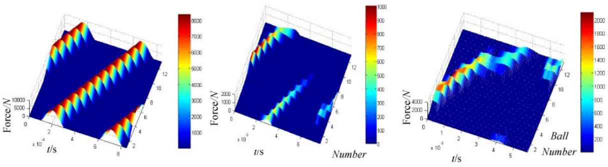

(d) 20600 rpm (e) 22500 rpm (f) 30000 rpm

Fig. 22. The changing law of the contact forces for each ball at different rotating speeds.

tion. In Figs. 20(c) and (d), the discrete spectrum appears in the casing acceleration frequency spectrum, that is, quasi-periodic phenomenon.

Figs. 21(a)-(c) show the orbits of the rotor and out ring, wave and frequency spectrum of the casing acceleration at the compressor rotor support S_2 when the rotating speed is 35000 rpm. In Fig. 21(a), due to the larger rotating speed, the contact force is larger, and the vibration of the out ring is bigger. In Figs. 21(b) and (c), the rotational frequency appears in frequency spectrum.

3.7 The nonlinear contact forces for each ball and the evolution of contact force for the rolling bearing

Figs. 22(a)-(f) show the evolution of contact forces for each ball when the radial clearance is 30μm at the support S_2, the contact time is one period of revolution of the rolling bearing cage and the ball number is 13. The evolution of contact forces for each ball changing with time and ball number can be seen in these figures. Figs. 22(a)-(d) show the rotor squeeze two balls, three balls, four balls and five balls every moment, respectively. Figs. 22(e) and (f) show the rotor squeezes the out ring now and then. It is found that the time of the rotor squeezing each ball is same in one period of revolution of the rolling bearing cage before the first order critical speed, the number is increasing with the increase of the rotating speed and the movement of the rolling bearing is periodic in Figs. 22(a)-(d), which belongs to the condition that the rotor always squeezes the out ring. Between the two critical speeds, the rotor squeezes the out ring now and then, the time of the rotor squeezing the out ring is different in one period of revolution of the rolling bearing cage, and the movement of the rolling bearing is quasi periodic and chaos in Figs. 22(e) and (f), that is instability phenomenon.

Figs. 23(a)-(f) show the evolution of the contact forces for the rolling bearing S_2. The evolution of the contact forces for the rolling bearing S_2 can be seen in these figures. Figs. 23(a)-(d) show the contact forces are increasing gradually and the contact forces for the rolling bearing S_2 are periodicity. Figs. 23(e) and (f) show the condition the rotor squeezes the out ring now and then and the contact forces for the rolling bearing S_2 are quasi periodicity and chaos.

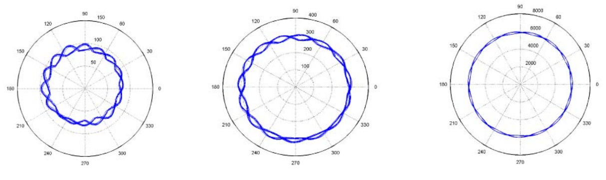

(a) 8000 rpm (b) 12000 rpm (c) 16100 rpm

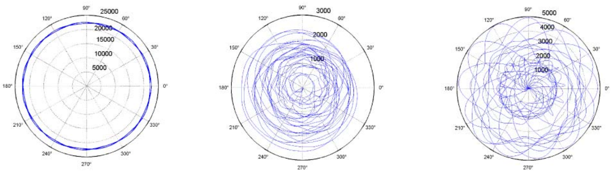

(d) 20600 rpm (e) 22500 rpm (f) 30000 rpm

Fig. 23. The changing law of the contact forces for the rolling-bearing at different speeds.

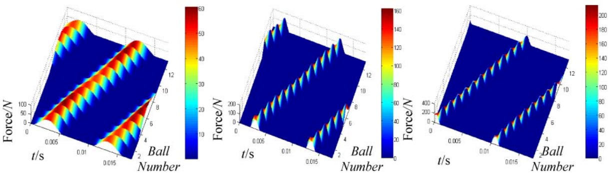

(a) 0 μm (b) 30 μm (c) 50 μm

Fig. 24. The changing law of the contact force for each ball in different radial clearances.

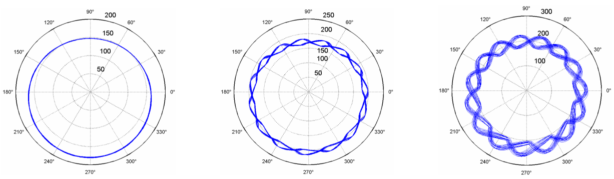

(a) 0 μm (b) 30 μm (c) 50 μm

Fig. 25. The changing law of the global contact forces for the rolling bearing in different radial clearances.

3.8 The influence of the radial clearance on the contact forces

In order to study the influence of the radial clearance on the contact forces, the evolution of contact forces for each ball and the global restoring forces for the rolling bearing S_2 are shown in Figs. 24 and 25 when the clearances are 0 μm, 30 μm and 50 μm, respectively. Figs. 24(a)-(c) show the rotor squeeze five balls, three balls, and two balls every moment, respectively. The number is decreasing with the increase of the radial clearances. Figs. 25(a)-(c) show the fluctuation of the global contact forces is high by the increase of the radial clearances.

4. Conclusion

In this paper, certain type real engine whole vibration model with the radial clearance of the rolling bearing is established, the strong nonlinearity of the radial clearance and the Hertz contact forces are considered in this model. The response of coupled system is obtained by numerical integration method. Some results are obtained as follows:

(1) The changing law of the casing acceleration amplitude with the rotating speeds is analyzed at different radial clearances. It is found that the jumping phenomenon is caused by the strength of nonlinearity of rolling bearing with the radial clearance. It shows that it can reduce the whole vibration and improve the rotor's stability by reducing the radial clearance.

(2) The characteristics of the casing acceleration response are analyzed with the radial clearance. In high rotating speed, duo to the variable stiffness of the rolling bearing, when the stiffness changes obviously, the rotor squeezes the out ring now and then, so the natural frequencies of the system are excited, that is *frequency-locked phenomenon*.

(3) The evolution of contact forces for each ball and the global contact forces at different rotating speeds are analyzed, and the rotor and the out ring load characteristics are analyzed. When the out ring is period loaded, the whole vibration is stabile. When the out ring is loaded now and then, the whole vibration is unstable.

(4) The influence of the radial clearance on the contact forces is analyzed. The contact forces will larger when the radial clearance is increased.

Acknowledgment

This work is supported by Funding of Jiangsu Innovation Program for Graduate Education KYLX_0295.

References

[1] F. F. Ehrich and J. J. O'Connor, Stator whirl rotors in bearing clearance, *ASME Journal of Engineering for Industry* (1967) 381-390.

[2] F. F. Ehrich, High order subharmonic response if high speed rotors in bearing clearance, *ASME Journal of Vibration, Acoustics, Stress and Reliability in Design*, 110 (1988) 9-16.

[3] J.-J. Sinou, Non-linear dynamics and contacts of an unbalanced flexible rotor supported on ball bearings, *Mechanism and Machine Theory*, 44 (2009) 1713-1732.

[4] S. P. Harsha, K. Sandeep and R. Prakash, Non-linear dynamic behaviors of rolling element bearings due to surface waviness, *Journal of Sound and Vibration*, 272 (2004) 557-580.

[5] S. P. Harsha, Nonlinear dynamic response of a balanced rotor supported by rolling element bearings due to radial internal clearance effect, *Mechanism and Machine Theory*, 41 (6) (2006) 688-706.

[6] M. Tiwari, K. Gupta and O. Prakash, Effect of a ball bearing on the dynamics of a balanced horizontal rotor, *Journal of Sound and Vibration*, 238 (5) (2000) 723-756.

[7] M. Tiwari and K. Gupta, Dynamics response of an unbalanced rotor supported on ball bearings, *Journal of Sound and Vibration*, 238 (5) (2000) 757-779.

[8] G. Jang and S. W. Jeong, Vibration analysis of a rotation system due to the effect of ball bearing waviness, *Journal of Sound and Vibration*, 269 (2004) 709-726.

[9] G. Chen, C. G. Li and D. Y. Wang, Nonlinear dynamic analysis and experiment verification of rotor-ball bearings-support-stator coupling system for aeroengine with rubbing coupling faults, *Journal of Engineering for Gas Turbines and Power*, 132 (2010) 022501-1/022501-9.

[10] B. Changqing and X. Qingyu, Dynamic model of ball bearings with internal clearance and waviness, *Journal of Sound and Vibration*, 294 (2006) 23-48.

[11] Aeroengine design manual compiling committee, *Aero-engine design manual 19th part: rotor dynamics and whole-engine vibration,* Beijing: Aviation Industry Press, 2000:208-226 (in Chinese).

[12] C. Guo, A coupling dynamic model for whole aero-engine vibration and its verification, *Journal of Aerospace Power*, 27 (2) (2012) 242-254 (in Chinese).

[13] W. M. Zhai, Two simple fast integration methods for large-scale dynamic problems in engineering, *International Journal for Numerical Methods in Engineering,* 39 (1996) 4199-4214.

[14] A. Muszynska, Whirl and whip rotor/bearing stability problems, *Journal of Sound and Vibration*, 110 (1986) 443-462.

[15] H. F. Wang and G. Chen, Certain type turbofan engine whole vibration model with support looseness fault and casing response characteristics, *Shock and Vibration* (2014) 1-23.

[16] H. F. Wang, G. Chen and P. P. Song, Asynchronous vibration response characteristics of aero-engine with support looseness fault, *Journal of Computational and Nonlinear Dynamics*, 11 (2016) 031013-1-031013-10.

[17] J. Wu, M. Legrand and C. Pierre, Non-synchronous vibration of a Jeffcott rotor due to internal radial clearance in roller bearings, *The 8th IFToMM International Conference on Rotor Dynamics*, KIST, Sep. 2010, Seoul, South Korea (2010) 446-453.

Haifei Wang is a Lecturer of College of Mechanical Engineering, Yangzhou University, Yangzhou, P. R. China. He is currently mainly engaged in the study of whole aero-engine vibration, rotor-bearing dynamics, rotating machine fault diagnosis, studying rotor-bearing dynamics, neural networks, and intelligent diagnosis.
E-mail: wanghaifei1986318@163.com.

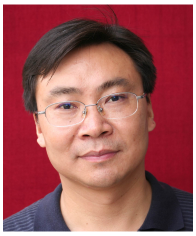

Junjie Gong is a Proffessor of College of Mechanical Engineering, Yangzhou University, Yangzhou, P. R. China. He is currently mainly engaged in the study of the dynamic and static test and optimization of the mechanical structure, and computer modeling and simulation of engineering problems.
E-mail: gjunj@126.com.

Guo Chen is a Professor at the College of Civil Aviation, Nanjing University of Aeronautics and Astronautics, Nanjing, P. R. China. He is currently mainly engaged in the study of whole aero-engine vibration, rotor-bearing dynamics, rotating machine fault diagnosis, pattern recognition and machine learning, and signal analysis and processing.
E-mail: cgzyx@263.net.